Journal of Materials Chemistry C

PAPER

View Article Online
View Journal | View Issue

Cite this: J. Mater. Chem. C, 2016, 4, 9516

Melanin-based flexible supercapacitors†

Prajwal Kumar,[a] Eduardo Di Mauro,[b] Shiming Zhang,[a] Alessandro Pezzella,[c] Francesca Soavi,[d] Clara Santato*[b] and Fabio Cicoira*[a]

Received 29th August 2016,
Accepted 20th September 2016

DOI: 10.1039/c6tc03739a

www.rsc.org/MaterialsC

Biocompatible and biodegradable materials that store electrochemical energy are attractive candidates for applications in bioelectronics and electronics for everywhere. Eumelanin is a ubiquitous biopigment in flora and fauna. It exhibits strong broad-band UV-visible absorption, metal chelation as well as good thermal and photo-stability. Eumelanin is based on 5,6-dihydroxyindole (DHI) and 5,6-dihydroxyindole carboxylic acid (DHICA) building blocks, present in different redox forms (hydroxyquinone, semiquinone and quinone). The synergy between the redox activity of the building blocks and the capability of several of their functionalities to reversibly bind cations constitutes the foundation for the use of melanin in pseudocapacitive energy storage systems. In this work, we report on the energy storage properties of eumelanin in supercapacitor configuration. Initially, a gravimetric specific capacitance as high as 167 F g^{-1} (specific capacity of 24 mA h g^{-1}) was observed for eumelanin on carbon paper electrodes, in aqueous electrolytes. A maximum power density of up to 20 mW cm^{-2} was deduced for the corresponding melanin supercapacitors. Capitalizing on these results, we used an unconventional patterning approach to fabricate binder-free flexible micro-supercapacitors on plastic substrates. Our results demonstrate that melanin is a valid candidate for future supercapacitor electrodes. The biocompatibility and biodegradability featured by eumelanin, combined with its easy availability and room temperature processing, make it an extremely attractive material for environmentally and human friendly energy storage solutions.

Introduction

Environmentally and human friendly electronic devices based on natural biocompatible and biodegradable materials are expected to benefit our everyday life, by improving our current capability to handle waste electrical and electronic equipment (WEEE) and boosting the development of smart environments for "ubiquitous sensor networks" and biomedical implants.[1,2]

Micro-supercapacitors are of the utmost importance to address the need for on-board energy supply/storage, *e.g.* in wearable electronic devices and embedded wireless sensor networks.[3–10] Supercapacitors, with respect to batteries, exhibit higher power density and longer cycle life.[11] Micro-supercapacitors are mostly fabricated from three classes of materials, *i.e.* carbon (activated carbon and nanostructured carbon), conducting polymers and metal oxides.[12] Micro-supercapacitors based on natural electrode materials and aqueous electrolytes, exhibiting mechanical flexibility, are of primary interest for environmentally and human friendly microelectronics for everywhere.[13–17]

Melanin is a ubiquitous biopigment in flora and fauna. It exhibits strong broad-band UV-visible absorption, metal chelation as well as good thermal and photo-stability. Different forms of melanin perform various functions in the human body, such as photoprotection (eumelanin) and hair and eye color (eumelanin and pheomelanin). Moreover, melanin pigments are also present in unexposed regions such as the inner ear and the substantia nigra of the brain.[18–20] The form of melanin most investigated by physicists and materials chemists is eumelanin (indicated henceforth as melanin for simplicity). Melanin is based on 5,6-dihydroxyindole (DHI) and 5,6-dihydroxyindole carboxylic acid (DHICA) building blocks (Scheme 1). The different redox forms of the building blocks, hydroxyquinone, semiquinone and quinone moieties, coexist in the macromolecular structure that results from the non-covalent interactions of nanoaggregates, which in turn ensue from the π–π stacking of planar sheets of the building blocks, of variable extent.[21,22] The macromolecular structure of melanin stabilizes the semiquinone and quinone (oxidized) redox forms of the building blocks. The quinone

[a] Department of Chemical Engineering, Polytechnique Montréal, C.P. 6079, Succ. Centre-ville, Montréal, Québec, H3C 3A7, Canada. E-mail: fabio.cicoira@polymtl.ca
[b] Department of Engineering Physics, Polytechnique Montréal, C.P. 6079, Succ. Centre-ville, Montréal, Québec, H3C 3A7, Canada. E-mail: clara.santato@polymtl.ca
[c] Dipartimento di Scienze Chimiche, Università di Napoli Federico II, Cupa Nuova Cintia, 21, 80126, Napoli, Italy
[d] Dipartimento di Chimica "Giacomo Ciamician", Alma Mater Studiorum – Universitá di Bologna, Via Selmi, 2, 40126, Bologna, Italy. E-mail: francesca.soavi@unibo.it

† Electronic supplementary information (ESI) available: Additional figures and related discussion, video of an operating flexible supercapacitor (MOV file). See DOI: 10.1039/c6tc03739a

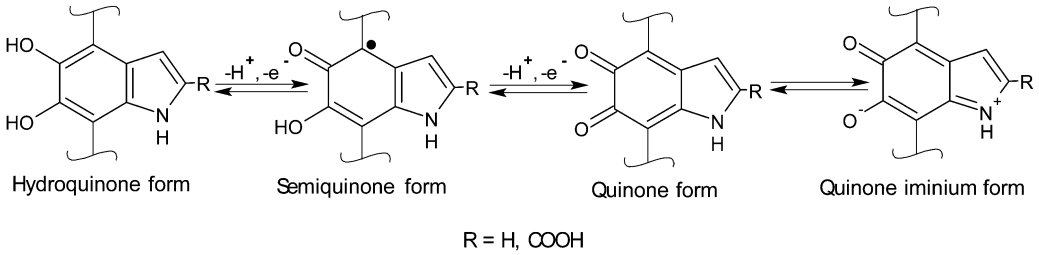

Scheme 1 Melanin building blocks DHI (R═H) and DHICA (R═COOH) and their redox forms hydroquinone (H_2Q), semiquinone (SQ) and quinone (Q); the quinone iminium (QI) form is the tautomer of quinone.

functionality of the molecule has the ability to store $2e^-/2H^+$ per quinone unit (Scheme 1).[11,23–25]

The synergy between the redox activity of the building blocks and the capability of several of their functionalities to reversibly bind cations constitutes the foundation for the use of melanin in pseudocapacitive energy storage systems. Unlike supercapacitors making use of carbon electrodes, which store energy by a purely electrostatic process, redox-active materials (pseudocapacitive materials) permit to exploit faradaic processes to achieve higher specific capacitance. The redox processes are accompanied by ion motion from/to the electrolyte into/from the redox active material. In melanin, carboxyl, amine, hydroxyl (phenolic), quinone and semiquinone moieties can serve as potential sites for metal cation accommodation.[26] Kim *et al.* reported catechol-mediated reversible binding of multivalent cations in melanin half-cells and, based on different affinities for multivalent cations of catechols and quinones, proposed that these cations bind to melanin *via* catechols and are extracted from melanin as catechol oxidizes into quinone. Functionalities other than catechols would likely have a minor effect on charge storage.[14,27,28] Studies of the generation and transport of charge carriers established that the electrical response of melanin strongly depends on its hydration state through a comproportionation equilibrium. In presence of water, hydroquinone and quinone moieties form charge carriers, protons and electrons (semiquinone extrinsic free radicals).[29,30] Recent studies by our groups contributed to the understanding of the proton conduction properties of melanin, in controlled humidity conditions.[31,32] Important findings on the ion transport properties of melanin have been reported in relation to its biological role in the human body, where melanin is believed to act as an ion storage and release medium.[18,26] For applications in electrochemical energy storage, the relatively low electrical conductivity of melanin (10^{-4}–10^{-3} S cm^{-1}) points to the need for efficient current collectors, such as electrically conductive carbon-based materials.[33,34]

Here we report on the use of melanin as electrode material for supercapacitors and micro-supercapacitors. The pseudocapacitive properties of melanin were initially studied using conductive carbon paper as current collector and then exploited to demonstrate, through the use of unconventional patterning, melanin-based flexible micro-supercapacitors. The main novelty of our work is the discovery of a new natural material for supercapacitor electrodes, besides well-established materials, such as activated carbons, carbon nanotubes, graphene, metal oxides and conducting polymers. Natural materials have already been used for the fabrication of supercapacitor electrodes. Nevertheless, in most cases, these materials have to be pyrolysed and activated to yield activated carbon electrodes, or they are mixed with conducting polymers to yield pseudocapacitive electrodes (see Table S1, ESI†).[35–53] Unlike these natural materials, our melanin can be simply deposited by solution processing at room temperature and does not require any thermal treatment or further mixing. The biocompatibility and biodegradability featured by melanin, together with its easy availability, make it an extremely attractive material for environmentally and human friendly energy storage solutions.[54]

Results and discussion

Cyclic voltammetry studies on melanin

The capability of melanin to store charge was initially assessed by cyclic voltammetry using electrodes consisting of melanin drop cast on conductive carbon paper (indicated henceforth with Mel/CP, see Experimental), exploiting the high mechanical stability of melanin on CP (Fig. 1 and Fig. S1, ESI†). As a matter of fact, we were able to run only 1–3 voltammetric cycles using melanin deposited on other types of electrodes, such as indium tin oxide (ITO). We investigated different electrolytes, in a typical three-electrode configuration, to assess the effect of the composition and pH of the electrolyte on the Mel/CP behavior. In $NH_4CH_3COO_{(aq)}$ at pH 5.5, the voltammetric response of Mel/CP electrodes with increasing melanin loadings (33.75 and 67.5 μg cm^{-2}, normalized with respect to the electrode footprint) shows that the current density increases with increasing loading (Fig. 1a). Our measurements also show that bare CP does not contribute significantly to the overall capacitance. The Mel/CP voltammograms are quasi box-shaped (rectangular). The absence of easily distinguishable voltammetric peaks is likely due to the convolution of several redox processes taking place at sites characterized by different molecular environments and different affinity to the electrolyte.[55] Indeed, melanin is a mixture of chemically similar biopolymers, rather than a well-defined chemical entity.[19] This chemical heterogeneity, coupled with limited solubility, made the characterization of melanin notoriously challenging over the years.[56]

The presence of melanin on CP was confirmed by Scanning Electron Microscopy (SEM) images obtained in back-scattered

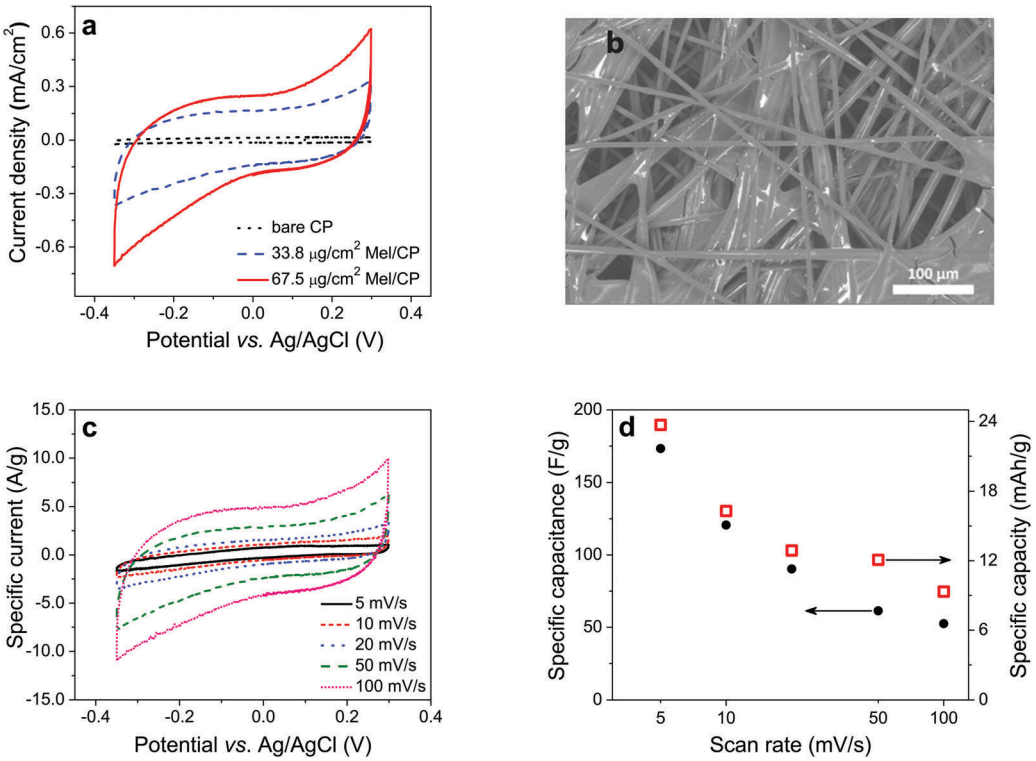

Fig. 1 (a) Cyclic voltammetry of 33.8 μg cm^{-2} and 67.5 μg cm^{-2} Mel/CP electrodes and bare carbon paper (CP, control sample) in $NH_4CH_3COO_{(aq)}$ pH 5.5; scan rate 50 mV s^{-1}. (b) SEM image, acquired in BSE mode, of a sample made of melanin on carbon paper (CP, loading of *ca.* 0.9 mg cm^{-2}) stained with uranyl acetate. The bright areas correspond to melanin chelating the uranyl oxycation. Acceleration voltage 10 kV. (c) Cyclic voltammetry of 33.8 μg cm^{-2} Mel/CP in $NH_4CH_3COO_{(aq)}$ pH 5.5 at different scan rates. (d) Specific capacitance and capacity *vs.* scan rate of Mel/CP electrodes (33.8 μg cm^{-2}), in $NH_4CH_3COO_{(aq)}$ pH 5.5. Geometric size of the samples 0.4 cm^2.

electron (BSE) mode (Fig. 1b). The intensity of the BSE signal is related to the atomic number. Melanin and CP are not distinguishable in BSE SEM images since they are constituted of carbon and other low-atomic number species. Therefore, to distinguish melanin from CP, we used staining with the salt uranyl acetate, exploiting the well-established property of melanin to chelate cationic species containing high atomic number metals, such as uranium.[26,57]

The voltammetric current of Mel/CP electrodes has a linear dependence on the scan rate ($i = C\frac{dV}{dt}$, Fig. 1c and Fig. S2, ESI,† where C is the capacitance) thus suggesting that the Mel/CP electrochemical behavior is pseudocapacitive. Notably, the electrically conducting network of CP permits values of the specific current (current normalized by melanin weight), as high as 5 A g^{-1}. The specific capacitance of the Mel/CP electrodes was obtained by normalizing, over the melanin loading, the slope of the plot of the integral of the cathodic current over time *vs.* electrode potential. The gravimetric specific capacity (storable charge per unit weight) was deduced from the cathodic current integrated over time and normalized by the melanin loading (Fig. 1d). At 5 mV s^{-1}, we obtained a specific capacitance of 167 F g^{-1} (*i.e.* 5.6 mF cm^{-2}), which well compares with values found on high surface area carbons, carbon nanotubes and graphene,[58] and a specific capacity of 24 mA h g^{-1}. The specific capacitance and capacity decrease with increasing scan rate, as expected for pseudocapacitive processes, which are affected by the rate of charge transfer/transport and mass transport (diffusion) of counter ions to/from the redox sites. However, faradaic side reactions, potentially contributing to the pseudocapacitive response, cannot be excluded at relatively low scan rates. From the comparison of the electrochemical behavior in different electrolytes, within a pH range compatible with the chemical stability of melanin (Fig. S3 and S4, ESI†),[59–61] we deduced that the best response is achieved for $NH_4CH_3COO_{(aq)}$ pH 5.5, in agreement with the well-established proton conduction properties of melanin (for the cycling stability of Mel/CP electrodes see Fig. S5, ESI†).[32] At pH 5.5, the currents in $NH_4CH_3COO_{(aq)}$ are higher than in $Na_2SO_{4(aq)}$ (this holds true for different $NH_4CH_3COO_{(aq)}$ concentrations). This result suggests possible specific effects of the ions constituting the electrolyte on the electrochemical behavior.[62] NH_4CH_3COO has acido-base properties possibly assisting proton transfer associated to electron transfer. Furthermore, aqueous solutions of the organic salt NH_4CH_3COO are expected to wet the melanin surface better than $Na_2SO_{4(aq)}$, thus promoting the access of the electrolyte to the melanin redox sites. Given that the highest specific capacitance was obtained with $NH_4CH_3COO_{(aq)}$, this electrolyte was selected for further studies of supercapacitors.

Melanin-based supercapacitors

The pseudocapacitive properties of Mel/CP electrodes were exploited to demonstrate supercapacitors based on identical

positive and negative Mel/CP electrodes, immersed in the electrolyte $NH_4CH_3COO_{(aq)}$ pH 5.5. Supercapacitors with different melanin loadings were characterized by galvanostatic charge/discharge cycles (Fig. 2). The profiles of the cell voltage and potentials of the individual electrodes during a galvanostatic charge/discharge cycle at 12.5 mA cm^{-2} (*i.e.* 92.6 A g^{-1}, considering the melanin loading of both electrodes) have a triangular shape. The coulombic efficiency (charge liberated during the discharge divided by charge accumulated during the charge) is 99.7% (Fig. 2a). These results demonstrate the good reversibility of the charge/discharge process.

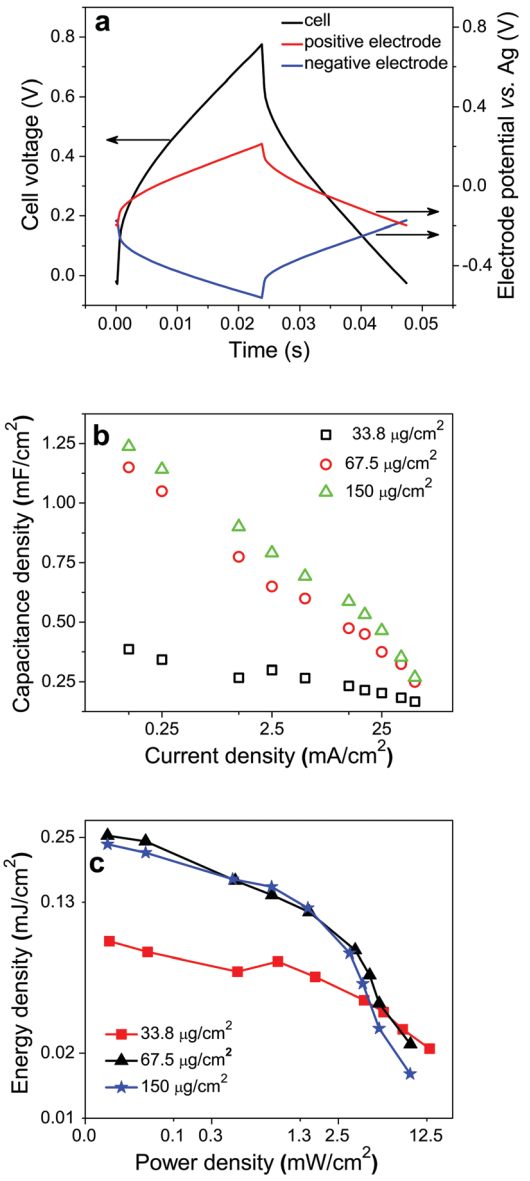

Fig. 2 Mel/CP supercapacitors with two identical Mel/CP electrodes of equal loadings and with $NH_4CH_3COO_{(aq)}$ pH 5.5 electrolyte. (a) Cell voltage and electrode potential profiles during a charge–discharge galvanostatic cycle (20th cycle) obtained at 12.5 mA cm^{-2} with 67.5 μg cm^{-2} Mel/CP (each electrode). (b) Capacitance density *vs.* current density, for three different melanin loadings. (c) Ragone plots extracted from galvanostatic discharge cycles for different melanin loadings with current density of 0.125, 0.25, 1.25, 2.5, 5, 12.5, 17.5, 25, 37.5 mA cm^{-2}.

The capacitance of the supercapacitor, evaluated from the reciprocal of the slope of the cell voltage over the charge liberated during the discharge, is of 0.48 mF cm^{-2} (*i.e.* 3.6 F g^{-1} considering the total melanin loading on the two electrodes). The corresponding maximum energy density, E_{max}, is 0.135 mJ cm^{-2} and the maximum power density, P_{max}, is 20 mW cm^{-2}, deduced from the relationships $E_{max} = \frac{1}{2}CV^2$ and $P_{max} = \left(\frac{V^2}{4 \times ESR}\right)$, where C is the cell areal capacitance, V is the cut off voltage (0.75 V) and ESR is the equivalent series resistance (6.8 Ω cm^2).[63]

The charge/discharge rate capability of supercapacitors with Mel/CP electrodes featuring different melanin loadings was investigated by galvanostatic charge/discharge cycles, run at different values of the current density (Fig. 2b). The capacitance density increased with the increase of the melanin loading from 33.8 to 67.5 μg cm^{-2}, whereas at 150 μg cm^{-2} the performance did not significantly improve, likely due to the relatively low melanin conductivity and to a more difficult access of the electrolyte to the electrode.[2,18] The supercapacitor with the lowest melanin loading featured the highest retention of the capacitance density that decreased by only 57% by increasing the current density by more than two orders of magnitude, *i.e.* from 0.125 up to 50 mA cm^{-2}.

The analysis of the galvanostatic discharge profiles for increasing values of the current density permitted to deduce the energy density ($E = I\int V \cdot dt$, in mJ cm^{-2}, where I is the current density) and the average power density ($P = E/\Delta t$ in mW cm^{-2}, where Δt is the discharge time) delivered during a complete discharge. The E and P values were in turn used to build Ragone plots, where the energy density is plotted *versus* the power density (Fig. 2c).[64–66] For a melanin loading of 33.8 μg cm^{-2} we obtained a relatively high value of the power density, *i.e.* up to 13.2 mW cm^{-2}, and a relatively low value of the energy density (highest value 0.08 mJ cm^{-2}). Supercapacitors with 67.5 μg cm^{-2} and 150 μg cm^{-2} loadings showed similar power density (highest value *ca.* 9.3 mW cm^{-2}) and energy density (highest value *ca.* 0.23–0.25 mJ cm^{-2}). These results point to the need of efficient and stable electrical contact between the melanin and the carbon current collector, further confirmed by the cycling performance of the supercapacitor (Fig. S6, ESI†).

We propose the following working principle for our melanin supercapacitors (Fig. 3). At the positive electrode, during charging (Fig. 3b), the redox active groups that are in the (semi) reduced form (semiquinone, SQ, and hydroquinone, H_2Q) are oxidized, thus leading to the increase of the concentration of quinone (Q) groups. At the same time, protons and ammonium cations are released in solution and anions (acetate) are incorporated in the electrode material. At the negative electrode, Q and SQ groups are reduced with an increase of the concentration of H_2Q groups. At the same time, anions are released in solution and protons and ammonium cations are incorporated in the electrode material. These processes are reversed during discharging (Fig. 3c).

With the aim to shed light on the evolution of the chemical features of our melanin-based electrodes after charging and discharging processes, we performed an X-ray photoelectron

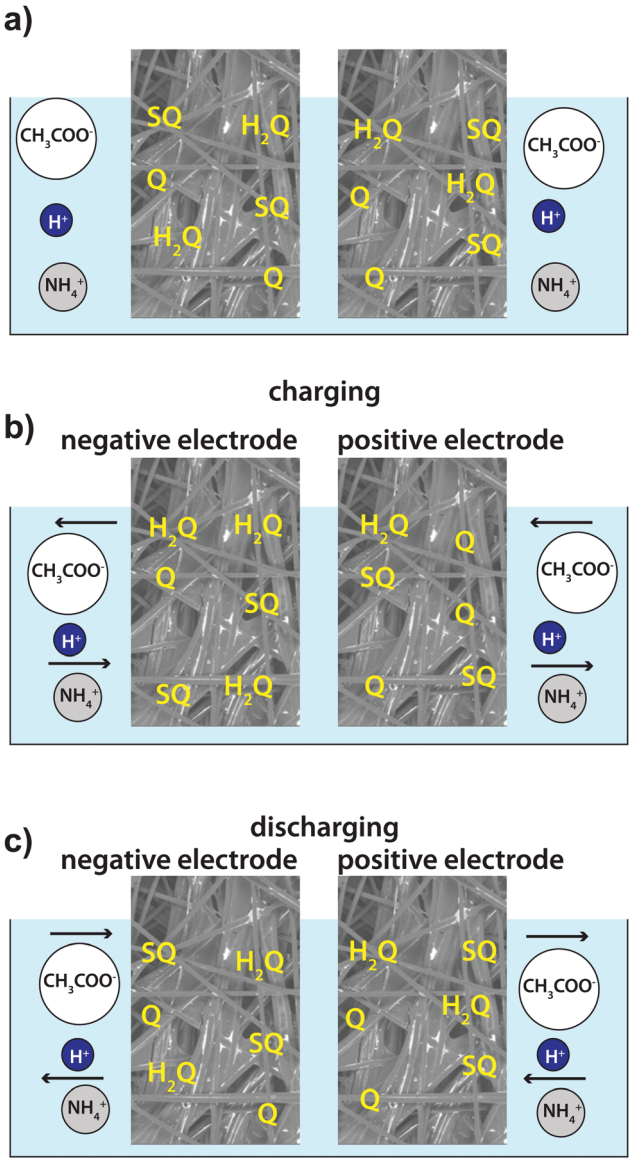

Fig. 3 Working principle of melanin-based supercapacitors constituted by two identical negative and positive electrodes, immersed in $NH_4CH_3COOH_{(aq)}$ pH 5.5. (a) Situation before a potential is applied between the electrodes, (b) situation produced during charging and (c) situation produced during the discharging of the electrodes. See Scheme 1 for the chemical structure of H_2Q, SQ and Q groups.

spectroscopy (XPS) study on the positive electrode of our supercapacitor. Although the results of the high resolution spectra did not permit to draw an exhaustive and detailed picture, nonetheless they permitted to deduce an increase of the C1s peak associated to the aromatic C═O bonding (binding energy of 287.4 eV), in agreement with the hypothesis of an increased concentration of quinone groups during the charging step (Table S2 and Fig. S7–S9, ESI†). No significant shift of the position of the N1s and O1s peaks was detected. Such a shift might have been attributed to the formation of new bonds involving O and N atoms, during the charging and discharging steps. The slight, but still significant, increase of the overall N1s concentration after charging with respect to discharging, can tentatively be attributed to the chemical affinity between melanin and NH_3.[62,67] Indeed, $NH_{4(aq)}^+$ is expected to be present as NH_3 in proximity of the positive electrode during the charging step.

Melanin-based micro-supercapacitors

The progress in electronics for everywhere calls for flexible and conformable microelectromechanical systems (MEMS) with integrated power sources. Flexible supercapacitors have generated enormous interest in the last years. A wide range of devices, based on several electrode/electrolyte combinations, fabricated with lithography or direct write techniques have been reported.[68–74]

We fabricated planar and binder-free micro-supercapacitors on flexible polyethylene terephthalate (PET) substrates (Scheme S1, ESI†) employing an unconventional and environmentally friendly microfabrication process based on parylene patterning (Fig. 4).[17,75–77] Pre-cleaned PET sheets (thickness of about 180 μm) were placed on a glass wafer pre-coated with a thin polydimethylsiloxane (PDMS) layer, to ensure flatness and rigidity during the following lithography steps. To facilitate parylene peel-off at the end of the patterning process, a cetyl trimethylammonium bromide (CTAB) solution was spin coated on PET prior to parylene coating. Successively, a 2 μm-thick ParyleneC film was deposited. A positive-tone photoresist was then spun onto parylene and a mask aligner was used to expose it through a photomask featuring the shape of the supercapacitor electrodes. After photoresist development, the unprotected parylene was etched by oxygen plasma and the unexposed photoresist was removed (see Experimental), to leave a patterned parylene layer, which acted as a mask for the patterning of the micro-supercapacitors. The electrode material of the micro-supercapacitors consisted of a composite layer

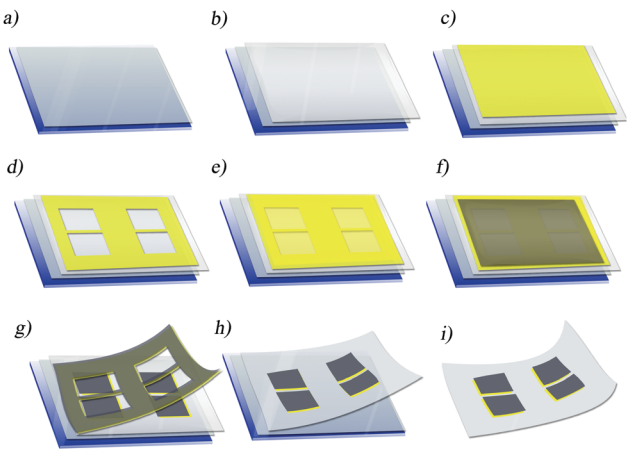

Fig. 4 Process flow for fabrication of micro-supercapacitors on flexible PET substrates: (a) a glass slide is covered with PDMS; (b) PET is laminated on the glass slide; (c) ParyleneC is deposited by chemical vapor deposition; (d) ParyleneC is patterned by photolithography and oxygen RIE to generate ParyleneC-free regions on PET; (e) Ti (4 nm) and Au (40 nm) are deposited by e-beam evaporation; (f) melanin/carbon black slurry is drop cast; (g) ParyleneC is peeled-off; (h) and (i) PET is removed from the glass slide to achieve the final flexible device.

of melanin and carbon black (Timcal Super C65, surface area 60 m^2 g^{-1}) drop-cast on evaporated Ti/Au current collectors (2 mm × 4 mm), with an electrode gap of 200 μm (see Experimental and Scheme S1, ESI†). After a thermal treatment, the parylene film was peeled off, leaving the patterned micro-supercapacitor (Fig. 5a). A PDMS or glass well was used to confine the electrolyte ($NH_4CH_3COO_{(aq)}$ pH 5.5).

From the voltammograms of micro-supercapacitors on PET (Fig. S10a and b, ESI†), we deduced the areal, volumetric and gravimetric specific capacitances (Fig. 5b and Fig. S10c, ESI†), at scan rates ranging from 0.01 V s^{-1} to 10 V s^{-1}. At a scan rate of 0.01 V s^{-1}, we deduced a gravimetric specific capacitance of 10.8 F g^{-1}, considering the total melanin loading on the two electrodes, and a specific capacity of 1.8 mA h g^{-1} (Fig. S10c, ESI†), whereas at 10 V s^{-1} corresponding values of 2.5 F g^{-1}, and 0.4 mA h g^{-1} were obtained. Areal and volumetric capacitances of 4.2 mF cm^{-2} and 1.7 F cm^{-3} were deduced at 0.01 V s^{-1} (Fig. 5b).

The rate response of the micro-supercapacitor was investigated by Electrochemical Impedance Spectroscopy (EIS). The Nyquist plot (Fig. S11a, ESI†) consists of a high frequency semicircle overlapped with a low frequency tail. The ESR estimated by the Z_r axis intercept of the plot at 100 kHz is 4.5 Ω cm^2. The high frequency semicircle is related to electron transfer processes that give rise to the capacitive response of the electrodes and to the contact resistance between melanin and carbon particles and between melanin and current collector. The areal impedance related to the high frequency semicircle is smaller than 4.5 Ω cm^2, which indicates the good electronic properties of the electrodes. The low frequency tail is almost parallel to the Z_i axis and is representative of the pseudocapacitive behavior of melanin. The Bode plot (Fig. S11b, ESI†), given in terms of capacitance normalized to the capacitance exhibited at 10 mHz, where capacitance is obtained at each frequency by the equation $C = 1/(Z_i 2\pi f)$, reveals a good frequency response of the micro-supercapacitor. Indeed, the micro-supercapacitor features a pseudocapacitive behavior starting from frequencies lower than *ca.* 1 kHz.

The galvanostatic charge/discharge characterization of micro-supercapacitors yielded a maximum capacitance of 2.1 mF cm^{-2} (*i.e.* 5.25 F g^{-1}) at 0.625 mA cm^{-2} (Fig. S12, ESI† and Fig. 5c) and an equivalent series resistance (ESR) of 6 Ω cm^2 that well compares with the value estimated by EIS. We obtained E_{max} and P_{max} of 0.6 mJ cm^{-2} and 23 mW cm^{-2}, calculated as previously discussed. The practical energy and power values were evaluated from the galvanostatic discharges at different current densities and reported in a Ragone plot (Fig. 5d): 0.44 mJ cm^{-2} and 5.24 mW cm^{-2} were the highest values deduced. Ragone plots where the performance of the micro-supercapacitor is normalized with respect to the volume or the area of the micro-supercapacitor are shown in Fig. S12b (ESI†).

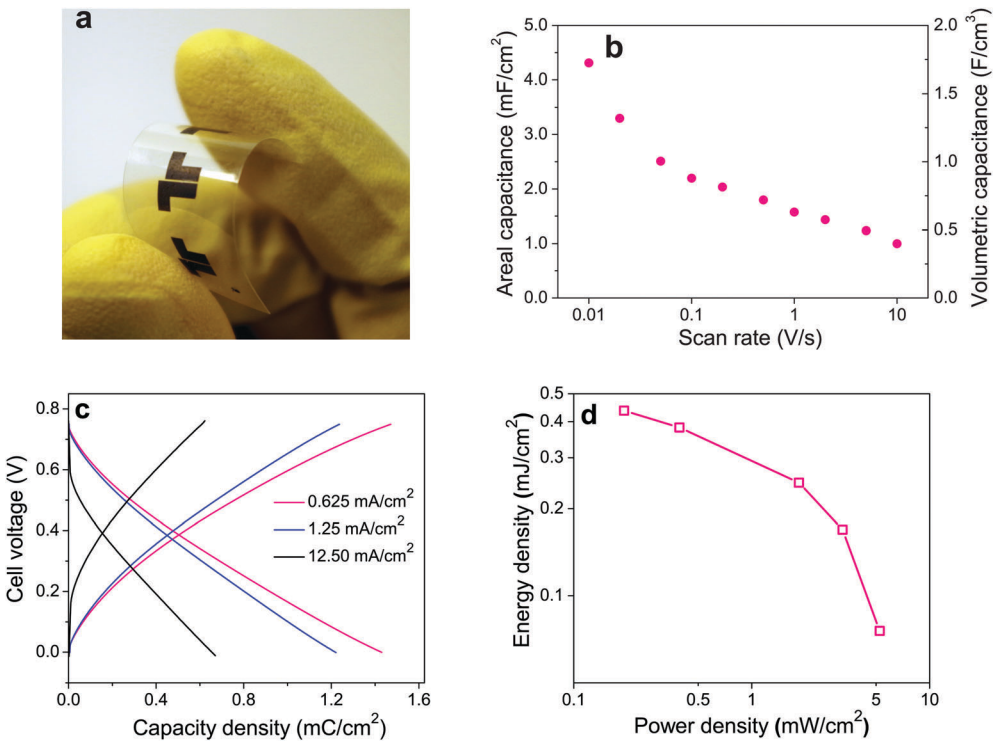

Fig. 5 Melanin-based flexible micro-supercapacitors with ~200 μg cm^{-2} melanin loading on each electrode using $NH_4CH_3COO_{(aq)}$ pH 5.5 as the electrolyte. (a) Optical image of the micro-supercapacitor (total three micro-supercapacitors) on a flexible PET substrate. (b) Areal capacitance and volumetric capacitance *vs.* scan rate of the cyclic voltammetry (obtained from Fig. S10a and b, ESI†) taking into account that the total area of the two electrodes is 0.16 cm^2 and that the corresponding volume is about 2 × 10^{-4} cm^3 (see Experimental). (c) Galvanostatic charge/discharge cycles with three different values of the current density (0.625, 1.25, and 12.5 mA cm^{-2}). (d) Ragone plot extracted from the galvanostatic discharge cycles at different values of the current density (0.625, 1.25, 6.25, 12.5 and 25 mA cm^{-2}). The area of each electrode is 0.08 cm^2.

Considering the typical thickness of about 12.5 μm for each of our electrodes, the volume of each electrode in the micro-supercapacitor is *ca.* 1×10^{-4} cm^3. Hence, E_{max} and P_{max} of the flexible melanin-based micro-supercapacitors, normalized to the volume of the two electrodes, are about 0.24 J cm^{-3} (68 μW h cm^{-3}) and 9.4 W cm^{-3}. In principle, our patterning process permits to microfabricate a "battery" of micro-supercapacitors on the same flexible substrate, thus enabling series/parallel connections for powering small electronics devices. As an example, the three series connected micro-supercapacitors of Fig. 5a could deliver a maximum power of 5.5 mW at 2.25 V. Our micro-supercapacitor showed 61% retention of the capacitance between the 500th and 20 000th cycle (Fig. S13, ESI†).

Within the same range, the supercapacitor showed a capacitance retention of about 40% (Fig. S6, ESI†). Despite the fact that a melanin-based supercapacitor is a totally new concept, and as such there is plenty of room to improve its performance, the values of the energy and power density, as well as device stability, compare reasonably well with the those of micro-supercapacitors based on more established materials.[3,58]

Preliminary tests performed on the melanin micro-supercapacitors show that no significant change of the voltammetric current occurs upon bending the micro-supercapacitors up to about 50% (Fig. S14, Scheme S2 and video file in the ESI†).[17] The capacitance contribution of carbon Super C-65 in micro-supercapacitors was evaluated by cyclic voltammetry analysis (Fig. S15, ESI†). The voltammograms show the higher capacitance of melanin/carbon C-65 compared to carbon Super C-65.

Conclusions

In summary, we demonstrated supercapacitors and flexible micro-supercapacitors making use of electrodes based on the biocompatible and biodegradable pigment melanin, working in aqueous electrolytes. Melanin-based supercapacitor electrodes are fabricated at room temperature, by easy solution processing, without the need of a high-temperature treatment, unlike the large majority of supercapacitors based on biopolymer-derived electrodes reported to date. In slightly acidic media, a gravimetric specific capacitance as high as 167 F g^{-1} (specific capacity of 24 mA h g^{-1}) was observed for melanin-based electrodes on carbon paper. A maximum power density of up to 20 mW cm^{-2} was deduced for the corresponding melanin supercapacitor. Capitalizing on these results, we demonstrated a binder-free micro-supercapacitor fabricated on flexible polyethylene terephthalate (PET). The microfabrication was performed by unconventional lithography based on ParyleneC patterning. Our flexible micro-supercapacitors showed a power density of 5.24 mW cm^{-2} at an energy density of 0.44 mJ cm^{-2} and a specific capacitance of 10.8 F g^{-1} (about 4.3 mF cm^{-2}, *i.e.* 1.7 F cm^{-3}). Micro-supercapacitors were operated at fast electrode potential scan rates (up to 10 V s^{-1}).

The performance of melanin micro-supercapacitors can be further improved by (i) using interdigitated finger structures with tuned electrode width, length, interelectrode distance and number of fingers and (ii) improving the formulation of the melanin slurry to optimize melanin loading. To achieve a better understanding about the redox sites active during the operation of the (micro-)supercapacitors, we are presently characterizing the electrochemical properties of chemically controlled melanins, *e.g.* obtained by the solid state polymerization of the DHI building blocks.[78] Our work paves the way to the fabrication of biodegradable/bioresorbable micro-supercapacitors using substrates such as poly(lactic-*co*-glycolic acid) (PLGA) or shellac and current collectors based on magnesium or iron alloys. Melanin based micro-supercapacitors may serve in biocompatible and biodegradable power sources for applications such as implantable medical devices, wearable electronics and ubiquitous sensor networks.

Experimental section

Materials

For the microfabrication process, we used glass slides (Corning), Polydimethylsiloxane (PDMS) Sylgard 184 from Dow Corning, PET sheets from Policrom Inc. (Bensalem, PA), CTAB from Sigma Aldrich and Parylene C from SCS Coatings. Photoresist SPR 220 3.0 and stripper PG 1165 were purchased from MicroChem. Developer AZ 726 was purchased from MicroChemicals. Eumelanin, phosphate buffered saline (PBS) tablets, ammonia buffer pH 10, sodium sulfate decahydrate ($Na_2SO_4 \cdot 10H_2O$) were purchased from Sigma-Aldrich. Ammonium acetate and dimethyl sulfoxide (DMSO) were purchased from Caledon Labs. All the materials were used as received. To prepare the solution of ammonium acetate $NH_4CH_3COO_{(aq)}$ pH 5.5, the salt was dissolved in water by sonication to obtain a concentration of 7.5 M and acetic acid was added to adjust the pH to 5.5 (other concentrations of ammonium acetate solutions, at pH 5.5, were also studied following an analogous procedure). The ionic conductivity of $NH_4CH_3COO_{(aq)}$ pH 5.5 was 60.5 mS cm^{-1} whereas that one of 0.5 M $Na_2SO_{4(aq)}$ pH 5.5 was 61.3 mS cm^{-1}. To prepare the PBS solution, one tablet was dissolved in 200 mL of deionized water. This yields 0.01 M phosphate, 0.0027 M potassium chloride and 0.137 M sodium chloride, pH 7.4, at 25 °C.

Fabrication of melanin electrodes on carbon paper (Mel/CP electrodes)

A melanin suspension in DMSO at 3 mg mL^{-1} was prepared by mixing in a planetary mixer (Thinky ARM-310) at 2000 rpm for 30 min. Three different loadings of the aforementioned suspension (33.8 μg cm^{-2}, 67.5 μg cm^{-2} and 150 μg cm^{-2}, normalized with respect to the electrode footprint) were applied by drop-casting melanin on carbon paper (CP, Spectracarb™ 2050A, 10 mils). After drop casting, the samples were dried at 50 °C under vacuum (*ca.* 40 mbar) for 2 h, to facilitate DMSO removal. Mel/CP electrode area is 0.4 cm^2.

Structures of the supercapacitors and micro-supercapacitors

For the supercapacitors, two identical electrodes of melanin on carbon paper (Mel/CP) were used as positive and negative

electrodes and Ag wire was used as quasi reference electrode. For the micro-supercapacitors, the positive and negative electrodes were made of melanin/carbon black composite (weight ratio 4/1, *i.e.* 16 mg of melanin and 4 mg of conductive carbon Super C-65 in 1 mL DMSO) deposited on Au electrodes (see below). The capacitive performance of carbon Super C-65 was evaluated by cyclic voltammetry in a three-electrode cell. Melanin/carbon Super C-65 (weight ratio 4/1–96 μg of melanin and 24 μg of carbon Super C-65) and pure carbon Super C-65 (24 μg) in DMSO were deposited on Au and used as working electrodes in the electrochemical cell. The electrode area was 0.36 cm^2.

Unconventional lithography steps for micro-supercapacitors on plastic

To fabricate flexible micro-supercapacitors on plastic, polyethylene terephthalate (PET) substrates were cleaned by sequential sonication in acetone, isopropanol, and de-ionized (DI) water, dried using a nitrogen flow and laminated on a cleaned glass wafer pre-covered with a polydimethylsiloxane (PDMS) adhesive layer, which was used to ensure the PET flatness and rigidity during the successive patterning steps. An aqueous solution of CTAB (10^{-3} M) was spun on PET to enable parylene delamination at the end of the process. The PET substrates were then transferred to a system for parylene-C deposition (SCS coating). After ParyleneC deposition, a positive tone photoresist (MEGAPOSIT SPR 220.3) was spin-coated on Parylene-C, then exposed to the UV light of the Karl Suss MA-6/BA-6 mask aligner (wavelength 365 nm) through a photomask and developed by immersion in AZ-726 to open windows on ParyleneC. The unprotected parylene-C was then etched by oxygen reactive ion etching (RIE) and the photoresist remaining on ParyleneC film was removed by immersing the samples in PG 1165 remover. Subsequently, 4 nm Ti and 40 nm Au were deposited on the patterned samples by E-beam evaporation, followed by a drop casting of melanin/carbon black slurry for micro-supercapacitors (see above). After a soft baking at 40 °C under vacuum (30 mm Hg for 20 minutes), the ParyleneC layer on PET was slowly peeled off, leaving patterned melanin micro-supercapacitors on PET. The fabrication process was completed by peeling-off PET from the PDMS/glass substrate. The area of each electrode is 0.08 cm^2, the thickness of the coating about 12.5 μm and the inter electrode distance is 200 μm (Scheme S1, ESI†).

Electrochemical set-up

Cyclic voltammetry (CV) was performed using a Versa STAT 3 potentiostat (Princeton Applied Research) in a three-electrode cell, where Mel/CP was the working electrode, Pt foil the counter electrode and $Ag/AgCl_{(aq)}$ the reference electrode. Galvanostatic charge/discharge cycles of the supercapacitor and micro-supercapacitor were performed using a Biologic VSP 300 multichannel potentiostat.

X-ray photoelectron spectroscopy (XPS)

High-resolution XPS analysis was carried out with a VG ESCALAB 3 MKII instrument under Mg Kα radiation by applying 300 W (15 kV, 20 mA) power. The pressure in the chamber during the analyses was 5.0×10^{-9} Torr. The high resolution spectra were acquired with a pass energy of 20 eV and electrons were collected at a 90 deg takeoff angle. Peak fitting was performed with symmetrical Gaussian–Laurentzian product functions after Shirley background subtraction. Wagner sensitivity factors were used to normalize the peak intensities for quantification.

Scanning Electron Microscopy (SEM)

SEM was performed at an acceleration voltage of 10 kV in backscattered electron (BSE) imaging mode using a FEI Quanta 450 Environmental Scanning Electron Microscope (FE-ESEM). Staining was achieved by exposing the samples (30 μL of a suspension of 12 mg mL^{-1} of melanin in DMSO poured on an area of 1 cm × 0.4 cm leading to a final loading of *ca.* 0.9 mg cm^{-2}) to an aqueous solution of uranyl acetate (2%) for 3 minutes followed by rinsing with deionized water for 5 minutes.

Acknowledgements

The authors are grateful to Y. Drolet, D. Pilon and C. Clement for technical assistance, to Prof. H. Vali and Dr S. K. Sears for SEM investigations and to Dr J. Lefebvre for XPS studies. Funding for this project was provided by grants NSERC Discovery (F. C. and C. S.), FRQNT Équipe (F. C. and C. S.) and FRQNT Établissement de Nouveau Chercheur (F. C.). S. Z. is grateful to NSERC for financial support through a Vanier Canada Graduate Scholarship. F. S. acknowledges financial support from Alma Mater Studiorum – Università di Bologna (Research Mobility Program) and the Embassy of Canada (2015 Canada-Italy Innovation Award). This work is supported by CMC Microsystems through the MNT Financial Assistance and CMC Solutions programs.

References

1 M. Irimia-Vladu, *Chem. Soc. Rev.*, 2014, **43**, 588–610.
2 P. Meredith, C. J. Bettinger, M. Irimia-Vladu, A. B. Mostert and P. E. Schwenn, *Rep. Prog. Phys.*, 2013, **76**, 034501.
3 M. Beidaghi and Y. Gogotsi, *Energy Environ. Sci.*, 2014, **7**, 867–884.
4 T. M. Dinh, K. Armstrong, D. Guay and D. Pech, *J. Mater. Chem. A*, 2014, **2**, 7170–7174.
5 A. Ferris, S. Garbarino, D. Guay and D. Pech, *Adv. Mater.*, 2015, **27**, 6625–6629.
6 D. Pech, M. Brunet, H. Durou, P. Huang, V. Mochalin, Y. Gogotsi, P. L. Taberna and P. Simon, *Nat. Nanotechnol.*, 2010, **5**, 651–654.
7 J. Chmiola, C. Largeot, P.-L. Taberna, P. Simon and Y. Gogotsi, *Science*, 2010, **328**, 480–483.
8 J. Maeng, C. Meng and P. P. Irazoqui, *Biomed. Microdevices*, 2015, **17**, 7.
9 K. Wang, W. Zou, B. Quan, A. Yu, H. Wu, P. Jiang and Z. Wei, *Adv. Energy Mater.*, 2011, **1**, 1068–1072.
10 C. Meng, J. Maeng, S. W. M. John and P. P. Irazoqui, *Adv. Energy Mater.*, 2014, **4**, 1301269.

11 D. Vonlanthen, P. Lazarev, K. A. See, F. Wudl and A. J. Heeger, *Adv. Mater.*, 2014, **26**, 5095–5100.
12 A. González, E. Goikolea, J. A. Barrena and R. Mysyk, *Renewable Sustainable Energy Rev.*, 2016, **58**, 1189–1206.
13 Y. J. Kim, W. Wu, S. E. Chun, J. F. Whitacre and C. J. Bettinger, *Proc. Natl. Acad. Sci. U. S. A.*, 2013, **110**, 20912–20917.
14 Y. J. Kim, W. Wu, S. E. Chun, J. F. Whitacre and C. J. Bettinger, *Adv. Mater.*, 2014, **26**, 6572–6579.
15 G. Milczarek and O. Inganas, *Science*, 2012, **335**, 1468–1471.
16 C. Dagdeviren, B. D. Yang, Y. Su, P. L. Tran, P. Joe, E. Anderson, J. Xia, V. Doraiswamy, B. Dehdashti, X. Feng, B. Lu, R. Poston, Z. Khalpey, R. Ghaffari, Y. Huang, M. J. Slepian and J. A. Rogers, *Proc. Natl. Acad. Sci. U. S. A.*, 2014, **111**, 1927–1932.
17 S. Zhang, E. Hubis, C. Girard, P. Kumar, J. DeFranco and F. Cicoira, *J. Mater. Chem. C*, 2016, **4**, 1382–1385.
18 P. Meredith and T. Sarna, *Pigm. Cell Res.*, 2006, **19**, 572–594.
19 M. d'Ischia, A. Napolitano, A. Pezzella, P. Meredith and T. Sarna, *Angew. Chem., Int. Ed. Engl.*, 2009, **48**, 3914–3921.
20 L. Zecca, C. Bellei, P. Costi, A. Albertini, E. Monzani, L. Casella, M. Gallorini, L. Bergamaschi, A. Moscatelli, N. J. Turro, M. Eisner, P. R. Crippa, S. Ito, K. Wakamatsu, W. D. Bush, W. C. Ward, J. D. Simon and F. A. Zucca, *Proc. Natl. Acad. Sci. U. S. A.*, 2008, **105**, 17567–17572.
21 A. A. R. Watt, J. P. Bothma and P. Meredith, *Soft Matter*, 2009, **5**, 3754–3760.
22 C. T. Chen, C. Chuang, J. Cao, V. Ball, D. Ruch and M. J. Buehler, *Nat. Commun.*, 2014, **5**, 3859.
23 E. Frackowiak, M. Meller, J. Menzel, D. Gastol and K. Fic, *Faraday Discuss.*, 2014, **172**, 179–198.
24 B. Huskinson, M. P. Marshak, C. Suh, S. Er, M. R. Gerhardt, C. J. Galvin, X. Chen, A. Aspuru-Guzik, R. G. Gordon and M. J. Aziz, *Nature*, 2014, **505**, 195–198.
25 (*a*) Y. Ding and G. Yu, *Angew. Chem., Int. Ed.*, 2016, **55**, 4772–4776; (*b*) C. R. DeBlase, K. Hernández-Burgos, J. M. Rotter, D. J. Fortman, D. dos, S. Abreu, R. A. Timm, I. C. N. Diógenes, L. T. Kubota, H. D. Abruña and W. R. Dichtel, *Angew. Chem., Int. Ed.*, 2015, **54**, 13225–13229.
26 L. Hong and J. D. Simon, *J. Phys. Chem. B*, 2007, **111**, 7938–7947.
27 H. Lee, N. F. Scherer and P. B. Messersmith, *Proc. Natl. Acad. Sci. U. S. A.*, 2006, **103**, 12999–13003.
28 N. Holten-Andersen, M. J. Harrington, H. Birkedal, B. P. Lee, P. B. Messersmith, K. Y. Lee and J. H. Waite, *Proc. Natl. Acad. Sci. U. S. A.*, 2011, **108**, 2651–2655.
29 A. B. Mostert, B. J. Powell, F. L. Pratt, G. R. Hanson, T. Sarna, I. R. Gentle and P. Meredith, *Proc. Natl. Acad. Sci. U. S. A.*, 2012, **109**, 8943–8947.
30 S. B. Rienecker, A. B. Mostert, G. Schenk, G. R. Hanson and P. Meredith, *J. Phys. Chem. B*, 2015, **119**, 14994–15000.
31 J. Wünsche, F. Cicoira, C. F. O. Graeff and C. Santato, *J. Mater. Chem. B*, 2013, **1**, 3836–3842.
32 J. Wünsche, Y. Deng, P. Kumar, E. Di Mauro, E. Josberger, J. Sayago, A. Pezzella, F. Soavi, F. Cicoira, M. Rolandi and C. Santato, *Chem. Mater.*, 2015, **27**, 436–442.
33 M. Lazzari, C. Arbizzani, F. Soavi and M. Mastragostino, *Supercapacitors*, Wiley-VCH Verlag GmbH & Co. KGaA, 2013, pp. 289–306.
34 M. Lazzari, M. Mastragostino and F. Soavi, *Electrochem. Commun.*, 2007, **9**, 1567–1572.
35 F. N. Ajjan, N. Casado, T. Rebis, A. Elfwing, N. Solin, D. Mecerreyes and O. Inganäs, *J. Mater. Chem. A*, 2016, **4**, 1838–1847.
36 L. Jiang, G. W. Nelson, S. O. Han, H. Kim, I. N. Sim and J. S. Foord, *Electrochim. Acta*, 2016, **192**, 251–258.
37 Y. Lva, L. Ga, M. Liu, W. Xiong, Z. Xu, D. Zhu and D. S. Wright, *J. Power Sources*, 2012, **209**, 152–157.
38 M. Genovese, J. Jiang, K. Lian and N. Holm, *J. Mater. Chem. A*, 2015, **3**, 2903–2913.
39 J. Hur, K. Im, S. W. Kim, U. J. Kim, J. Lee, S. Hwang, J. Song, S. Kim, S. Hwang and N. Park, *J. Mater. Chem. A*, 2013, **1**, 14460–14466.
40 Q. Wang, Q. Cao, X. Wang, B. Jing, H. Kuang and L. Zhou, *J. Power Sources*, 2013, **225**, 101–107.
41 M. Biswal, A. Banerjee, M. Deo and S. Ogale, *Energy Environ. Sci.*, 2013, **6**, 1249–1259.
42 C. Wang, M. J. O. Connell and C. K. Chan, *ACS Appl. Mater. Interfaces*, 2015, **7**, 8952–8960.
43 L. Zhu, F. Shen, R. L. Smith, Jr. and X. Qi, *Energy Technol.*, 2016, **4**, 1–10.
44 X. Wang, D. Kong, Y. Zhang, B. Wang, X. Li, T. Qiu, Q. Song, J. Ning, Y. Song and L. Zhi, *Nanoscale*, 2016, **8**, 9146–9150.
45 D. H. Nagaraju, T. Rebis, R. Gabrielsson, A. Elfwing, G. Milczarek and O. Inganäs, *Adv. Energy Mater.*, 2014, **4**, 1300443.
46 L. Wei, M. Sevilla, A. B. Fuertes, R. Mokaya and G. Yushin, *Adv. Energy Mater.*, 2011, **1**, 356–361.
47 S.-K. Kim, Y. K. Kim, H. Lee, S. B. Lee and H. S. Park, *ChemSusChem*, 2014, **7**, 1094–1101.
48 C. Falco, J. M. Sieben, N. Brun, M. Sevilla, T. Mauelen, E. Morallon, D. Cazorla-Amoros and M.-M. Titirici, *ChemSusChem*, 2013, **6**, 374–382.
49 E. Raymundo-Piñero, F. Leroux and F. Béguin, *Adv. Mater.*, 2006, **18**, 1877–1882.
50 E. Raymundo-Piñero, M. Cadek and F. Béguin, *Adv. Funct. Mater.*, 2009, **19**, 1032–1039.
51 L. Yuan, C. Feng, C. Wang, Z. Fu, X. Yang and Y. Tang, *J. Mater. Sci.*, 2016, **51**, 3880–3887.
52 B. Xu, S. Hou, F. Zhang, G. Cao, M. Chu and Y. Yang, *J. Electroanal. Chem.*, 2014, **712**, 146–150.
53 K. Wang, R. Yan, N. Zhao, X. Tian, X. Li, S. Lei, Y. Song, Q. Guo and L. Liu, *Mater. Lett.*, 2016, **174**, 249–252.
54 C. J. Bettinger, A. Misra, J. T. Borenstein and R. Langer, *Biomaterials*, 2009, **17**, 3050–3057.
55 S. Gidanian and P. J. Farmer, *J. Inorg. Biochem.*, 2002, **89**, 54–60. The difference between the shape of the cyclic voltammograms in ref. 55 with respect to our voltammograms in Fig. 1 can be attributed to different factors: (i) in ref. 55 the voltammograms refer to the electropolymerization of the chemically defined DHI building blocks on gold disk electrodes whereas, in our case, we deal with drop-cast samples on carbon paper, deposited from suspensions of

commercially available eumelanin polymers; (ii) in ref. 55 the cyclic voltammogram of poly-DHI is run at a sweeping rate as slow as 0.5 mV sec^{-1} while we performed CV within the range 5–100 mV s^{-1}; (iii) the electrolyte used in ref. 55 for poly-DHI, is a phosphate buffer pH 7.0 including KCl 0.1 M (K^+ is a cation with a strong binding affinity for melanin), different from our work.

56 M. d'Ischia, K. Wakamatsu, F. Cicoira, E. Di Mauro, J. C. Garcia-Borron, S. Commo, I. Galvan, G. Ghanem, K. Kenzo, P. Meredith, A. Pezzella, C. Santato, T. Sarna, J. D. Simon, L. Zecca, F. A. Zucca, A. Napolitano and S. Ito, *Pigm. Cell Melanoma Res.*, 2015, **28**, 520–544.

57 T. Sakaguchi and A. Nakajima, *J. Chem. Technol. Biotechnol.*, 1987, **40**, 133–141.

58 G. Xiong, C. Meng, R. G. Reifenberger, P. P. Irazoqui and T. S. Fisher, *Electroanalysis*, 2014, **26**, 30–51.

59 A. J. Bard and L. R. Faulkner, *Electrochemical Methods: Fundamentals and Applications*, Wiley, 2nd edn, 2000.

60 P. Kumar, Z. Yi, S. Zhang, A. Sekar, F. Soavi and F. Cicoira, *Appl. Phys. Lett.*, 2015, **107**, 053303.

61 A. Sarapuu, K. Vaik, D. J. Schiffrin and K. Tammeveski, *J. Electroanal. Chem.*, 2003, **541**, 23–29.

62 P. Prem, K. J. Dube, S. A. Madison and J. Bartolone, *J. Cosmet. Sci.*, 2003, **54**, 4395–4409.

63 The maximum power is deduced from $P_{max} = \left(\frac{V^2}{4 \times ESR}\right)$ where the equivalent series resistance (ESR) is ESR = $\Delta V/2I$, with ΔV the initial drop in voltage upon switching from charging to discharging and I the current.

64 H. D. Abruna, Y. Kiya and J. C. Henderson, *Phys. Today*, 2008, **61**, 43–47.

65 B. E. Conway, *Electrochemical Supercapacitors-Scientific Fundamentals and Technological Applications*, Springer, 1999.

66 T. Brousse, D. Belanger and J. W. Long, *J. Electrochem. Soc.*, 2015, **162**, A5185–A5189.

67 J. P. Bothma, J. de Boor, U. Divakar, P. E. Schwenn and P. Meredith, *Adv. Mater.*, 2008, **20**, 3539–3542.

68 W. Liu, C. Lu, X. Wang, R. Y. Tay and B. K. Tay, *ACS Nano*, 2015, **9**, 1528–1542.

69 Y. Lim, J. Yoon, J. Yun, D. Kim, S. Y. Hong, S.-J. Lee, G. Zi and J. S. Ha, *ACS Nano*, 2014, **8**, 11639–11650.

70 Q. Jiang, N. Kurra and H. N. Alshareef, *Adv. Funct. Mater.*, 2015, **25**, 4976–4984.

71 D. Kim, G. Lee, D. Kim and J. S. Ha, *ACS Appl. Mater. Interfaces*, 2015, **7**, 4608–4615.

72 D. Qi, Z. Liu, Y. Liu, W. R. Leow, B. Zhu, H. Yang, J. Yu, W. Wang, H. Wang, S. Yin and X. Chen, *Adv. Mater.*, 2015, **27**, 5559–5566.

73 J. Liu, L. Zhang, H. B. Wu, J. Lin, Z. Shen and X. W. Lou, *Energy Environ. Sci.*, 2014, **7**, 3709–3719.

74 J. Liu, J. Sun and L. Gao, *J. Phys. Chem. C*, 2010, **114**, 19614–19620.

75 I. Kymissis, C. D. Dimitrakopoulos and S. Purushothaman, *J. Vac. Sci. Technol.*, 2002, **20**, 956–959.

76 J. D. Slinker, J. A. DeFranco, M. J. Jaquith, W. R. Silveira, Y.-W. Zhong, J. M. Moran-Mirabal, H. G. Craighead, H. D. Abruna, J. A. Marohn and G. G. Malliaras, *Nat. Mater.*, 2007, **6**, 894–899.

77 F. Cicoira, M. Sessolo, O. Yaghmazadeh, J. A. DeFranco, S. Y. Yang and G. G. Malliaras, *Adv. Mater.*, 2010, **22**, 1012–1016.

78 A. Pezzella, M. Barra, A. Musto, A. Navarra, M. Alfè, P. Manini, S. Parisi, A. Cassinese, V. Criscuolo and M. d'Ischia, *Mater. Horiz.*, 2015, **2**, 212–220.